Highly sensitive and stable fructose self-powered biosensor based on a self-charging biosupercapacitor

Bollella, Paolo; Boeva, Zhanna; Latonen, Rose-Marie; Kano, Kenji; Gorton, Lo; Bobacka, Johan

Published in:
Biosensors and Bioelectronics

DOI:
10.1016/j.bios.2020.112909

Published: 15/03/2021

Document Version
Accepted author manuscript

Highly Sensitive and Stable Fructose Self-Powered Biosensor based on a Self-Charging Biosupercapacitor

Paolo Bollella,[a] *Zhanna Boeva,*[a] *Rose-Marie Latonen,*[a] *Kenji Kano,*[b] *Lo Gorton,*[c,]* *Johan Bobacka*[a,]*

[a]Laboratory of Molecular Science and Engineering, Faculty of Science and Engineering, Johan Gadolin Process Chemistry Centre, Åbo Akademi University, Biskopsgatan 8, FIN-20500 Turku-Åbo, Finland

[b]Division of Applied Life Sciences, Graduate School of Agriculture, Kyoto University, Sakyo, Kyoto 606-8502, Japan

[c]Department of Analytical Chemistry/Biochemistry, Lund University, P.O. Box 124, 221 00, Lund, Sweden

Abstract

Herein, we present an alternative approach to obtain a highly sensitive and stable self-powered biosensor that was used to detect D-fructose as proof of concept.In this platform, we perform a two-step process, *viz*. self-charging the biosupercapacitor for a constant time by using D-fructose as fuel and using the stored charge to realize the detection of D-fructose by performing several polarization curves at different D-fructose concentrations. The proposed BSC shows an instantaneous power density release of 17.6 mW cm^{-2} and 3.8 mW cm^{-2} in pulse mode and at constant load, respectively. Moreover, the power density achieved for the self-charging BSC in pulse mode or under constant load allows for an enhancement of the sensitivity of the device up to 10 times (3.82 ± 0.01 mW cm^{-2} mM^{-1}, charging time = 70 min) compared to the BSC in continuous operation mode and 100 times compared to the normal enzymatic fuel cell. The platform can potentially be employed as a self-powered biosensor in food or biomedical applications.

Corresponding Authors e-mail lo.gorton@gmail.com, jbobacka@abo.fi

Keywords: self-powered biosensors, self-charging biosupercapacitors, fructose dehydrogenase, conducting polymers, enzyme-based electrodes.

1. Introduction

In the last decades, much progress in the bioelectrochemistry of redox enzymes has been achieved through the synthesis/electrosynthesis of new nanomaterials to enhance the efficiency of direct electron transfer (DET) between electrodes and a number of sugar oxidising enzymes (e.g. cellobiose dehydrogenase (CDH), pyranose dehydrogenase (PDH), fructose dehydrogenase (FDH), PQQ-dependent glucose dehydrogenase (PQQ-GDH) etc.) (Adachi et al., 2019; Bollella et al., 2018b; Bollella and Gorton, 2018; Gorton, 2020; Lisdat, 2020; Mano,

2019; Okuda-Shimazaki et al., 2020; Peterbauer, 2020; Scheiblbrandner and Ludwig, 2020). Besides the evolution of the electrode construction, one of the most intriguing achievement was reported in 2001 by Willner and Katz, who coined the new definition of "self-powered biosensors" correlating the power generation with different glucose concentrations (Katz et al., 2001). In particular, this definition merges two different fields, *viz*. biofuel cells (BFCs) and biosensors (Hickey et al., 2016; Yang et al., 2013). The latter category usually confers to the use of a three-electrode conventional cell containing a working bioelectrode, a reference and an auxiliary electrode, performing the analysis through the correlation between the variation of the catalytic current with different substrate concentrations (Roy et al., 2020; Fu et al., 2018; Grattieri and Minteer, 2018). Conversely, BFCs are operating with two bioelectrodes (an anode and a cathode), which are usually connected with a resistance load. In the biosensing field, most of the present day research is focused on increasing the sensitivity, selectivity and stability, while for BFCs, a large open circuit voltage (OCV), large short circuit currents and high power output densities represent the most important challenges (Falk et al., 2012; Leech et al., 2012). While considering the BFCs, it should be highlighted that the performance of the currently developed devices is really low by both energy density and power density means. Moreover, the performance could be limited when BFCs are implanted, where also biological limits should be taken into account (Shleev, 2017; Xiao et al., 2019). Therefore, a new class of bioelectronics was put forward, namely biological supercapacitors (or biosupercapacitors), a type of device belonging to the family of biosensors, bioelectronic circuitry, and BFCs (Kizling et al., 2015; Shleev et al., 2017; Xiao and Magner, 2018). Kizling and co-workers realized a device based on three air–fructose biofuel cells connected in series. The device was employed as a powering unit for a laboratory designed two-electrode minipotentiostat and a laccase based sensor for oxygen sensing (Kizling et al., 2015). In a similar approach, Xiao and Magner reported the realization of a quasi-solid-state and flexible biofuel cell using a hydrogel electrolyte preloaded with sugar as a fuel (Xiao and Magner, 2018). Moreover, Villarubia et al. obtained a paper based enzymatic fuel cell is used as self-recharged supercapacitor. In this supercapacitive enzymatic fuel cell (SC-EFC), the supercapacitive features of the electrodes are exploited to demonstrate high power output under pulse operation (Villarubia et. al., 2016). In biosupercapacitors, nanomaterials (*e.g.*, conducting polymers, gold nanoparticles (AuNPs), carbon nanotubes, graphene *etc.*) are used to prepare the charge storing component, where the charge is harvested through the action of the redox/metallic centers in the redox proteins immobilized on the anode/cathode electrodes (Alsaoub et al., 2017; Pankratov et al., 2014b, 2016). Beyond the conventional biosupercapacitors, a great progress in the field is certainly

represented by the construction of the first self-charging biosupercapacitor realized by Shleev's research group, where the charge storing component was realized with a polyaniline/multiwalled carbon nanotube (MWCNT) composite, while the electrochemical electromotive force to drive the charging process was accomplished by immobilizing CDH on the anode and bilirubin oxidase (BOx) on the cathode (Santoro et al., 2019b; Pankratov et al., 2014a). Both electrodes were based on AuNPs modified graphite electrodes. The initial-specific power was 1.2 mW cm^{-2} at 0.38 V (170 times the result reported for the BFC itself) delivered into a 500 Ω load, with quite a significant power being supplied for at least 50 min (Santoro et al., 2019b; Pankratov et al., 2014a).

Herein, we used FDH as the biocomponent on the anode and laccase on the cathode for the construction of the biosupercapacitive device. FDH from *Gluconobacter japonicus* has been largely exploited to develop DET based biosensors (Adachi et al., 2020). FDH from *Gluconobacter japonicus* consists of three subunits which are the catalytic dehydrogenase domain, DH_{FDH} (subunit I), where D-fructose is oxidised at a covalently bound flavin adenine dinucleotide cofactor (FAD), donating $2e^-$ that are transferred sequentially from $FADH_2$ to the cytochrome domain (CYT_{FDH}, subunit II) through an internal electron transfer (IET) mechanism. Subunit II consists of three heme *c* moieties coordinated by the enzyme scaffold, and a subunit III that is not involved in the ET process (Bollella et al., 2018c, 2018d, 2019). Connection with the anode then occurs directly from the CYT_{FDH}. Laccase from *Trametes versicolor* contains four copper atoms: the T1 copper site acts as an electron acceptor (DET configuration: electrons donated from the electrode), in this case the cathode, and mediated electron transfer (MET) configuration: electrons donated from a diffusing or immobilized mediator). Electrons are thereafter transferred through an IET mechanism to the T2/T3 trinuclear copper cluster where O_2 is reduced to H_2O (Bollella et al., 2018a; Momeni et al., 2019; Shleev et al., 2005; Zumpano et al., 2020). These redox enzymes should be electrically connected to different nanomaterials (*e.g.,* carbon nanotubes) through electrostatic interactions, a covalent linkage etc., in order to provide an efficient ET process. To this extent, multiwalled carbon nanotubes (MWCNTs) can be modified by using aromatic compounds to correctly orientate the enzymes on their surface or redox polymers to achieve maximum electron transfer efficiency. In particular, polymers with redox active side groups, such as osmium or iron complexes or polymers with intrinsic conductivity like polypyrrole (PPy) or polyaniline (PANI) have successfully been used (Bartlett and Birkin, 1993; Heller, 1992; Ramanavičius et al., 2006; Ruff, 2017; Yuan and Minteer, 2019; Zamani et al., 2019).

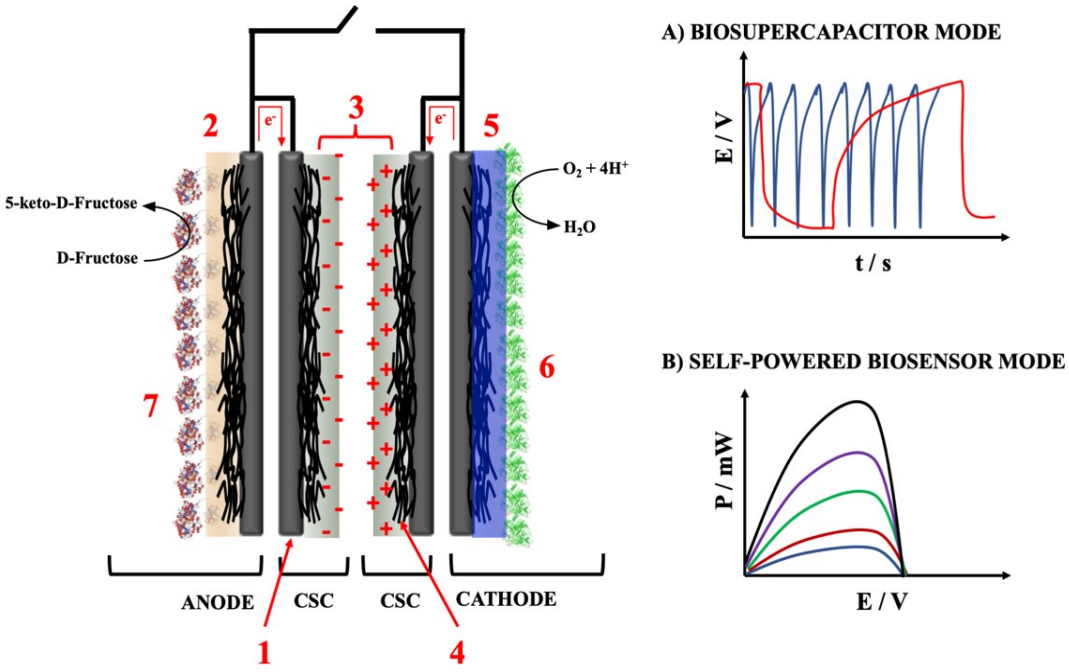

Scheme 1. Schematic representation of an enzyme-based biosupercapacitor during the charging process. 1: graphite electrodes; 2: poly-(2-aminobenzoic acid) (PABA); 3: poly-(aniline) (PANI); 4: multiwalled carbon nanotubes (MWCNT); 5: diazonium salt of 2-amino-anthracene; 6: laccase; 7: fructose dehydrogenase (FDH); CSC, charge storing components of bioelectrodes. The enzyme-based biosupercapacitor can work either as (A) biosupercapacitor or (B) self-powered biosensor.

In the present work, we aim at proving a novel concept in electroanalytical chemistry realizing to the best of our knowledge the first self-charging biosupercapacitor used as a self-powered biosensor for the detection of D-fructose. In this novel platform, we performed a two-step process: 1) self-charging the biosupercapacitor for a constant time by using D-fructose as fuel and 2) use the stored charge to realize the detection of D-fructose by performing several polarization curves at different D-fructose concentrations, Scheme 1 (Conzuelo et al., 2018). Notably, we were able to increase the sensitivity of the self-powered biosensor 100 times compared to the same conventional BFC operating as a self-powered biosensor. Besides sensitivity, also operational stability and reusability were improved with this biosensor configuration as well as the possibility to power the device without using any potentiostat/sourcemeter.

2. Experimental

2.1 Chemicals and Materials

D-Fructose, sodium acetate (NaAc), aniline (ANI), 2-aminobenzoic acid (ABA), sulfuric acid (H_2SO_4), 2-aminoanthracene (2-ANT), multi-walled carbon nanotubes (MWCNT, >98% carbon basis, O.D. × L 6-13 nm × 2.5-20 μm), hydrochloric acid (HCl) and sodium nitrite ($NaNO_2$) were purchased from Sigma Aldrich (St. Louis, MO, USA). D-Fructose dehydrogenase from *Gluconobacter japonicus* (FDH; EC 1.1.99.11) was purified according to previously reported procedure (Bollella et al., 2018d) (volumetric activity measured with potassium ferricyanide at pH 4.5 = 420 ± 30 U mL^{-1}, specific activity = 250 ± 30 U mg^{-1}, protein concentration = 1.7 ± 0.2 mg mL^{-1}). Fungal laccase from *Trametes versicolor* (*Tv*L) was supplied by Sigma Aldrich (EC 1.10.3.2, activity: 12.6 U mg^{-1}) and stored at −18 °C. Aqueous solutions were prepared with freshly deionized water deionized water of 18.2 MΩ·cm resistivity obtained with an ELGA purelab ultra water system.

2.2 Preparation of bioanode

Prior to use, graphite rods (Alfa Aesar GmbH & Co KG, AGKSP grade, ultra "F" purity, and 3.05 mm diameter, Karlsruhe, Germany) were polished on wet emery paper (Turfbak Durite, P1200) and rinsed with Milli-Q water. Afterwards, the graphite rods were inserted into a peek cylinder used as insulating material (put at the same level) to get a planar graphite disk electrode with a diameter of 3.05 mm. Next, 6 μL of a multiwalled carbon nanotube suspension (MWCNT suspension with a concentration of 10 mg mL^{-1} in 70:30 distilled H_2O:ethanol) were drop-cast onto the graphite disk electrode surface and let to dry at room temperature (3 h). Electropolymerization of poly-2-aminobenzoic acid aniline was performed by applying potentiostatic pulses (potentiostatic pulse electrodeposition method), Figure S1 (Fusco et al., 2017; Schubart et al., 2012).

During the optimization of the potentiostatic pulse electrodeposition method, several parameters were varied such as: oxidation potential (0.6, 0.7, and 0.8 V vs. Ag|AgCl|3M KCl), oxidation pulse time (0.4, 0.8, and 1.6 s), reduction potential (-0.1, -0.3, and -0.5 V vs. Ag|AgCl|3M KCl), reduction pulse time (0.1, 0.2, and 0.6 s), total electrodeposition time (100, 300, 600, 900, and 1400 s) and concentration of 2-aminobenzoic acid (25, 50, 100, and 500 mM) in 1 M H_2SO_4.

After preliminary experiments, the optimized electrode platform, namely PABA/MWCNT/G, was further washed with 5 mM MES buffer at pH 6 for 30 min in order to remove any monomer traces from the electrode. Next, 3 μL of an FDH solution (FDH enzyme was disolved in PBS buffer pH 6 (50 mM) containing 0.1 mM 2-mercaptoethanol and 0.1% v/v Triton X-100 used as enzyme stabilizer) was drop-cast onto the modified electrode and let dry at room temperature

(3 h). Finally, the electrode, namely FDH/PABA/MWCNT/G, was gently rinsed with 50 mM NaAc buffer at pH 5 and stored at 4 °C overnight.

2.3 Preparation of cathode

After a cleaning procedure (reported in the previous section), 6 µL of a MWCNT suspension (10 mg mL^{-1} in 70:30 distilled H_2O:ethanol) was cast onto the graphite disk electrode. Afterwards, the so modified electrode (G/MWCNT) was modified through the electrodeposition of 2-aminoanthracene (2-ANT) diazonium cation *in situ* generated, as previously reported (Bollella et al., 2018d).

Afterwards, 3 µL of a *Tv*L solution (solubilized in 10 mM NaAc buffer pH 4.5) was drop-cast onto the modified electrode and let to dry at room temperature (3 h). Finally, the electrode was gently rinsed with 50 mM NaAc buffer at pH 5 and stored at 4°C overnight.

2.4 Charge-storing components (CSC) preparation

After mechanical cleaning by using wet emery paper, the graphite disk electrodes were modified through drop-casting of 6 µL of a MWCNT suspension (10 mg mL^{-1} in 70:30 distilled H_2O:ethanol). Afterwards, electropolymerization of aniline (ANI) was performed by using the potentiostatic pulse method under the following experimental conditions: oxidation potential (0.9 V vs. Ag|AgCl|3M KCl), oxidation pulse time (0.8 s), reduction potential (-0.1 V vs. Ag|AgCl|3M KCl), reduction pulse time (0.2 s), total electrodeposition time (200, 400, and 600 s) and concentration of aniline (100 mM). The experimental conditions were selected based on a previous optimization reported for the bioanode preparation except for the oxidation potential that was varied to obtain a conductive polyaniline (PANI) layer, and the electrodeposition time that was also varied in order to obtain CSC elements with different capacitances (Fusco et al., 2017; Schubart et al., 2012).

2.5 Electrochemical characterization

Cyclic voltammetry, linear sweep voltammetry, charge/discharging (chronopotentiometry by application of current pulses, 100 µA for 3 s) and potentiostatic pulse experiments (chronoamperometry) were performed by using an Autolab PGSTAT 100 (Eco Chemie, Utrecht, The Netherlands) controlled by GPES Manager program v. 4.9 (Eco Chemie). Electrochemical impedance spectroscopy (EIS) experiments were performed by using a PGSTAT 30 potentiostat (Eco Chemie) controlled by Nova v. 2.1 (Eco Chemie). All electrochemical experiments were carried out in a conventional three electrodes cell equipped

with graphite disks (d= 3.05 mm) as working electrode, Ag|AgCl|3M KCl (BASi, West Lafayette, IN, USA) as reference (all potential values reported in the manuscript are referred to Ag|AgCl|3M KCl) and a graphite slab as counter electrode. Linear sweep voltammetry (LSV) experiments at slow scan rate (1 mV s^{-1}) from the open circuit potential (OCV) to 0 V were performed to record the polarization curves for the EFC configuration. The electrodes were connected considering the bioanode FDH/PABA/MWCNT/G as working electrode and the biocathode *Tv*L/2-ANT/MWCNT/G as a combined reference and counter electrode. In the biosupercapacitor (BSC) configuration, the charge storing components (CSCs) were short-circuited with the bioelectrocatalytic electrodes. Notably, PANI/MWCNT/G electrodes with different capacitances were used. The charge/discharge curves were recorded using a digital multimeter (BTMETER, BT-90EPC equipped with USB interface) applying an external load of 250 Ω.

2.6 Morphological and spectroscopic characterization

Scanning electron microscopy (SEM) measurements were performed with a LEO 1530 Gemini FE-SEM (Zeiss, Oberkochen, Germany). All samples were prepared according to the protocol reported above in the section "Bioanode preparation" and "charge-storing component (CSC) preparation" by using graphite plates (25 x 25 x 1 mm, ALS Co. Ltd., Tokyo, Japan) instead of graphite rods. The samples were placed on a clip SEM sample holder (Zeiss).

The UV-Vis measurements were performed by using an indium tin oxide (ITO) electrode (cat. CEC007, Präzisions Glas. & Optik GmbH, Iserlohn, Germany) to prepare PANI and PABA electropolymerized electrodes. All electrodes were placed in a plastic cuvette filled with 1 M H_2SO_4 and the UV–vis spectra were recorded (between 300 and 900 nm) with a Hitachi U-3900/3900H spectrophotometer (Tokyo, Japan).

Raman measurements were performed with the 514 nm laser (LaserPhysics, Ar ion laser) and 784 nm laser (Diode laser) for PABA and PANI, respectively, connected to a Renishaw Ramascope (system 100 equipped with the Wire™ v1.3 Raman software) equipped with a Leica DMLM imaging microscope and connected to a CCD camera. The spectrometer was calibrated using a Si-standard (520.0 cm^{-1}). The Raman spectrum of each composite film was recorded using 1% of the maximum laser power (20 mW for 514 nm laser and 28 mW for 784 nm laser) and accumulating 10 spectra.

3. Results and discussion

3.1 Morphological and spectroscopic characterization of PABA and PANI modified MWCNT/G electrodes

The surface features of the electrodeposited polymers were morphologically evaluated by taking SEM pictures of bare MWCNTs and of the polymer modified MWCNTs, Figures 1A-E. The polymer deposition preferentially occurred at the MWCNTs as hotspot, thus assuming a nanofiber structure for short electropolymerization times (PABA t_{exp}= 300 s and PANI t_{exp}= 200 s). By increasing the electropolymerization time up to 400 and 600 s for PANI, the polymer was covering the whole electrode.

UV–vis spectroscopy is one of the main tools used in characterizing conducting polymers. PANI has five stable forms known as leucoemeraldine, emeraldine and emeraldine salt, and pernigraniline and pernigraniline salt (Chiang and MacDiamid, 1986; Huang. et al., 1986). Each form has its known bands in the UV–vis spectrum. For example, emeraldine has two bands at 310-330 nm and 610-630 nm (Abaci et al., 2014). These peaks represent the $\pi \rightarrow \pi^*$ transition of the benzenoid (B) segment and the $\pi \rightarrow \pi^*$ transition of the quinoid (Q) segment, respectively. When pernigraniline is protonated two additional bands are acquired, one at 400–440 nm corresponding to a cation-radical and the band at 610-630 nm shifts towards >700 nm due to delocalization of the cation-radicals along the polymer backbone (polaron) (Cao, 1990; Yoon et al., 2011). Figure 2A shows the UV-vis spectra for PANI modified ITO electrodes obtained by using different electropolymerization times. In particular, an aniline monomer solution in 1 M H_2SO_4 did not show any band in the range 300-900 nm (black curve). Conversely PANI/ITO samples obtained with t_{exp}= 200, 400, and 600 s (red, blue and magenta curves) showed two bands at 440 nm and 720 nm, respectively, confirming the presence of protonated and electrically conducting polyaniline (Rahy and Yang, 2008). The bands exhibited an increased optical density for a higher amount of PANI electrodeposited onto the ITO electrodes. On the other hand, PABA did not show the polaron band probably due to its low to negligible conductivity, Figure 2B (red curve), as it was already discussed above during the electrochemical characterization. However, a 2-aminobenzoic acid solution in 1 M H_2SO_4 (black curve) showed a typical band for $\pi \rightarrow \pi^*$ transition of the phenyl ring (Karami et al., 2012).

To further elucidate the structural features of the PANI/MWCNT/G electrodes, Raman spectroscopy measurements were performed, Figure 2C. The spectrum for MWCNT/G (magenta curve) showed the characteristic D (D stands for ‘disorder’) and G (G stands for ‘graphite’) bands at 1279 and 1564 cm^{-1}, respectively (Heise et al., 2009). Both bands are in good agreement with results reported in the literature (Bulusheva et al., 2008; Costa et al.,

2008). The D and G bands of MWCNTs are not visible in the PANI spectra because the resonantly enhanced PANI bands in the same region overlap the D and G bands. Only a shoulder of the band at 1564 cm^{-1} is visible in the PANI/MWCNT/G spectra. The Raman spectra of PANI/MWCNT/G electrodes (t_{exp}= 200, 400, 600 s) show mostly the vibrational bands of the emeraldine salt (ES) form (black, red and blue curve, respectively) due to the resonance enhancement from the laser excitation wavelength used. The PANI t_{exp}= 600 s/MWCNT/G electrode (black curve) showed also a high background signal probably because of an increased fluorescence from the thick PANI film, which hides the structural features of the polymer more than with the thinner films. The main ES vibrational bands of PANI/MWCNT are located at 792 cm^{-1} for t_{exp}= 200, 400 s and 833 cm^{-1} for t_{exp}= 600 s (ring symmetric stretching; amine deformation, B) (Berrada et al., 1995; Furukawa et al., 1988; Lindfors and Latonen, 2014), 1143 cm^{-1} for t_{exp}= 200, 400 s and 1147 cm^{-1} for t_{exp}= 600 s (C-H in-plane bending, B) (Berrada et al., 1995; Furukawa et al., 1988; Lindfors and Latonen, 2014; Quillard et al., 1995). The 1307 cm^{-1} band for t_{exp}= 200 and 400 s (1319 cm^{-1} for t_{exp}= 600 s) is characteristic for C-N^{+} stretching of the radical cation. The broad band at around 1580 cm^{-1} includes the band at 1600 cm^{-1} characteristic for C-C ring stretching, B, the band at 1581 cm^{-1} (for t_{exp}= 200 and 400 s) and at 1571 cm^{-1} (for t_{exp}= 600 s) characteristic for C=C ring stretching, Q, and the contribution from the EB domains at 1477 cm^{-1} (for t_{exp}= 200, 400 s) and at 1475 cm^{-1} (for t_{exp}= 600 s) characteristic for C=N and CH=CH stretching, Q (Bartonek et al., 1990; Berrada et al., 1995; Furukawa et al., 1988; Lindfors and Latonen, 2014; Quillard et al., 1995).

3.2 Electrochemical characterization of bioanode FDH/PABA/MWCNT/G combined with different charge storing components (CSC)

FDH from *Gluconobacter japonicus* was immobilized onto MWCNT modified with electropolymerized poly-2-aminobenzoic acid (PABA) as conducting polymer (CP). After a complete characterization of the CP modified electrode used as bioanode (fully reported in the Supporting Information, SI), cyclic voltammetry (CV) measurements were carried out to investigate the bioelectrocatalytic properties of the FDH/PABA/MWCNT/G electrode, Figure 3A. CV curves were registered in the absence (in 50 mM NaAc buffer at pH 5, Figure 3A, black curve) and in the presence of 10 mM D-fructose (Figure 3A, red curve) showing a difference in current density of 411 ± 16 μA cm^{-2} measured at 0.4 V vs. Ag|AgCl|3M KCl. This increase is probably due to the electrochemical features of the CP, based on PABA, promoting the electron transfer (ET) pathway from FDH to the electrode surface. In particular, the increase in the ET rate could be related to the electrostatic attraction between FDH (positively charged at pH 5,

considering its isoelectric point (pI) at ~ 6.5 as from the enzymatic structure) (Bollella et al., 2018e) and the PABA layer (slightly negative as the positive charge located at the quinone-diimine nitrogen atoms is exceeded by the negative charge of the -COOH groups (pK_a= 4.95)) (Brett and Thiemann, 2002; Lindfors and Ivaska, 2002; Schuhmann et al., 1997; Wiklund and Bergman, 2006). Moreover, two couples of redox waves can be highlighted in both CVs, the first redox pair ($E^{0\prime}$= -0.080 V) is related to the conversion of the reduced form of polyaniline (leucoemeradine) to the mixed state (emeraldine) and the second one ($E^{0\prime}$= 0.225 V) is the redox conversion from emeraldine to the oxidized one (pernigraniline) (Schubart et al., 2012). The FDH/PABA/MWCNT modified graphite electrode (G) showed a capacitance density of 1.6 ± 0.2 mF cm^{-2} (all current and power densities in this work are calculated based on the bioanode area) was registered for the FDH/PABA/MWCNT modified graphite electrode (G) in the absence of D-fructose. The complete bioanode was assembled by connecting (short-circuiting) the charge storing components (CSCs) with various capacitances in parallel with the basic bioanode electrode. The electrochemical properties of CSCs modified by electropolymerizing aniline (different potentiostatic pulse schemes) was investigated in detail (data and description reported in the SI). Increasing the capacitance of the CSCs from 0 mF (bioanode without CSC) to 1.2 mF resulted in an 8 times increase in the bioelectrocatalytic current density, Figure 3B. However, any further increase in the CSC capacitance did not improve the bioelectrocatalytic performance of the complete bioanode.

Moreover, electrochemical impedance spectroscopy (EIS) measurements were performed to investigate the ET process occurring at the electrode, Figure 3C, ($\chi^2 < 10^{-3}$ for all experiments). The equivalent circuit reported in Figure D was adopted to fit EIS data. The equivalent circuit consists of ohmic resistance of the electrolyte (R_s), resistance to the charge transfer (R_{CT}), constant phase element accounting for the charge separation of the electrical double layer (CPE_{DL}) and the constant phase element for the electrode polarization (CPE_P). Notably, any increase in the capacitance of the CSC led to a decrease in R_s from 1942 ± 16 Ω (bioanode without CSC) to 380 ± 5 Ω for the bioanode containing the CSC with a capacitance of 1.2 mF. All data obtained from fitting EIS spectra with the aforementioned equivalent circuit are reported in Table S1. It is possible to observe as CPE_{DL} is increasing with the nominal capacitance or thickness of PANI layer, as well as CPE_P that is related with the combination of the biocatalytic electrode and the capacitive electrode. While the capacitive contribution was increasing, the contribution of faradaic processes remains constant, thus evidencing a decreasing of the R_{CT}. However, a similar type of behaviour has been reported for biosolar and microbial fuel cells, where additional capacitive electrodes were connected to a

bioelectrocatalytic electrode (Gonzalez-Arribas et al., 2017; Houghton et al., 2016; Pankratova et al., 2017; Santoro et al., 2016b; Soavi and Santoro, 2020). In addition, also the R_{CT} value decreased from 13.7 ± 0.6 to 0.238 ± 0.034 kΩ when connecting the CSC of 1.2 mF to the FDH bioanode, which indicates an enhancement in electron shuttling through the conducting layer of PABA.

3.3 Electrochemical characterization of biocathode TvL/2-ANT/MWCNT/G

Thereafter, the FDH bioanode was connected with a laccase modified electrode (cathode) in order to realize a BFC working as a self-powered biosensor for the detection of D-fructose, as schematically shown in Figure 4A. Laccase from *Trametes versicolor* (*Tv*L) was efficiently immobilized onto a MWCNT modified electrode as previously reported in the literature (Blanford et al., 2009). *Tv*L/2-ANT/MWCNT/G electrocatalytic behaviour was investigated in 50 mM NaAc buffer at pH 5, by scanning the electrode in anaerobic conditions (black curve) and in equilibrium with air (red curve), respectively, Figure S8. From both experiments, it was possible to observe an efficient electrocatalytic process occurring (difference in current density of 254 ± 9 μA cm^{-2} measured at 0 V *vs.* Ag|AgCl|3M KCl) starting at E_{onset} = 0.445 V *vs.* Ag|AgCl|3M KCl, Figure S6. The electrocatalytic wave might be ascribed to the selective orientation of *Tv*L onto the electrode surface through the hydrophobic region nearby the T1 site, thus enhancing the electron transfer rate to *Tv*L.

3.4 Enzymatic fuel cell and self-charging biosupercapacitor characterization

The open circuit voltage (OCV) of the assembled BFC was 0.524 ± 0.009 V, Figure 4B. The OCV was calculated (Figure S9B, black curve) as a result of the subtraction between open circuit potential (OCP) of cathodic electrode (*Tv*L/2-ANT/MWCNT/G, Figure S9A, blue curve) and the OCP of anodic electrode (FDH/PABA/MWCNT/G, Figure S9A, red curve) in presence of 20 mM D-fructose. In addition, the OCP of CSC electrode (Figure S9A, purple curve) was also reported as 0.028 ± 0.004 V, which is lower compared to the formal potential ($E^{0'}$= +0.128 V) related to conversion of the leucoemeraldine salt (LES) to the emeraldine salt (ES) form of PANI (Figure S4). The conversion of the leucoemeraldine salt (LES) to the emeraldine salt (ES) form of PANI is a 2H+/2e- process (Karami et al., 2012). Moreover, multiple polarization curves were measured by varying the concentration of D-fructose from 0 to 25 mM (Figure S10), obtaining a maximum power output density of 0.28 ± 0.01 mW cm^{-2} at a cell voltage of 0.3 V, Figure 4B, which is higher than other BFCs previously reported in the literature (Kamitaka et al., 2007; Kizling et al., 2016; So et al., 2014). The current example

exhibited a poor operation stability with a loss of almost 80% of its initial power density within the first 9 h, Figure 4C, thus hindering any possible employment to develop either biosensing or energy devices. Besides the operational stability, also the sensitivity over operation time of the self-powered fructose biosensor has been investigated, displaying a sensitivity drop of 75% after 2 h of operation compared to the initial sensitivity (0.058 ± 0.004 mW cm^{-2} mM^{-1}), Figure 4D.

To drastically increase the performance of the self-powered fructose biosensor, CSC electrodes (with a capacitance of 1.2 mF) were electrically connected in parallel (short-circuited) with the biocatalytic electrodes, *i.e.* the FDH bioanode and the *Tv*L biocathode, Figure 4E. The OCV of the assembled BSC remained almost unchanged (0.520 ± 0.007 V), while the maximum power output density resulted in a 10 times higher value compared to the basic BFC, notably 4.78 ± 0.12 mW cm^{-2} at a cell voltage of 0.41 V, Figure 4F, obtained from the polarization curves reported in Figure S11. The shift of the cell voltage corresponding to the maximum power output is ascribed to the addition of CSC electrodes short-circuited with the FDH bioanode and the *Tv*L biocathode, thus increasing the internal resistance between the bioelectrocatalytic electrodes (Liang et al., 2007). Additionally, the operational stability drastically increased retaining up to 90% of its initial power density after 8 h of continuous operation, Figure 4G. Similarly, the sensitivity increased by ~6.5 times (0.372 ± 0.011 mW cm^{-2} mM^{-1}, BSC operating in continuous mode), with a minimal loss after 2 h of operation (90 % of initial sensitivity retained), Figure 4H.

The self-charging features of the BSC was investigated either in pulse mode or by applying a constant load (250 Ω), Figure 5A. The stabilization of the OCV at ~0.5 V corresponds to the fully charged BSC composed of the bioanode equipped with a CSC element (open circuit potential (OCP) value of -0.084 ± 0.006 V, after addition of D-fructose) and the biocathode equipped with a CSC element (OCP value of 0.418 ± 0.009 V), Figure S12. The discharging of the BSC was performed by applying a constant current of 100 μA for 3 s to discharge the device, which results in a voltage drop of 0.43 V (corresponding to an instantaneous power density delivery of 17.6 mW cm^{-2}), followed by a recharging step up to the OCV value, Figure 5A (black curve). The charging/discharging process in pulse mode was performed 8 times showing a good stability. This result is in good agreement with other enzyme and microbial self-charging BSCs (Pankratov et al., 2018; Villarrubia et al., 2016; Xiao and Magner, 2018). The performance of the BSC was also tested by applying a constant load of 250 Ω during different charging/discharging cycles, 70/50 and 200/100 min, respectively, Figure 5A. In the first case, after OCV stabilization at 0.5 V a constant load of 250 Ω was applied over 50 min observing a

voltage drop of 0.39 V, which corresponds to an instantaneous power density delivery of 4.6 mW cm^{-2}, Figure 5A (red curve). Notably, the power density delivered instantaneously is reduced by almost 4 times compared to the discharging in pulse mode, probably due to the voltage decrease over time during the discharging process. During the second charging process, the voltage stabilized at 0.395 V over 70 min (a lowering of ca. 25% of the OCV initially registered). Next, the same load (250 Ω) was applied for 50 min, observing a voltage drop of 0.34 V (instantaneous power density delivery of 3.8 mW cm^{-2}). In the third cycle, the voltage was stabilized at 0.327 V over 70 min, a value substantially lower than the OCV (lower *ca.* 30%), suggesting a certain device stability over multiple charging/discharging processes. In fact, applying the same load (250 Ω) over 50 min, a voltage drop of 0.24 V was observed, which corresponds to an instantaneous power density delivery of 2.1 mW cm^{-2}. The stability of the device over multiple charging/discharging cycles could be ascribed to the biodegradation of the biocatalytic electrodes during the operation of the self-charging device. Thereafter, a load of 250 Ω was applied for a longer time (100 min) showing similar voltage drops of 0.405 V and 0.272 V in the first and second cycle, respectively, Figure 5A (green curve). The power density delivered instantaneously is further reduced by almost 15 times (1.3 mW cm^{-2}), thus not showing any long term stability. A comparison of the results obtained for the self-charging biosupercapacitor with those obtained by other researchers with different combinations of redox enzymes has been reported in Table S2 (Agnès et al., 2014; Bobrowski et al., 2018; Kizling et al., 2015; Villarubia et al., 2016). The system herein presented appears more complex (4 electrodes instead of 2 electrodes). Moreover, we achieved a maximal power output that is in good agreement with the ones obtained with different combinations of redox enzymes. In this regard, we should highlight that different enzymes exhibit different kinetics and interfacial electron transfer features, which makes hard the comparison between the platforms reported.

3.5 Self-powered biosensor characterization

After exploring the self-charging properties, the proposed self-charging BSC was used to detect D-fructose as a self-powered biosensor either in pulse mode or applying a constant load (250 Ω), Figure 5B. Besides the promising operational stability, also the sensitivity of the self-powered fructose biosensor over charging time has been investigated, displaying a sensitivity increase up to 10 times (3.82 ± 0.01 mW cm^{-2} mM^{-1}, charging time = 70 min) compared to the sensitivity observed in continuous operation mode, Figure 5B. The sensitivity was calculated based on the power output measured during the charging time (Figure S13) according to the following equation (Equation 1):

$(Q_{delivered}/t_{charge})$ x $(V_{ohmic} + V_{capacitive})$ (Eq. 1)

considering t_{charge}= 30 mins (1800 s), i_{pulse}= 100 μA, t_{pulse} = 3 s, ΔV_{ohmic} = 0.2 V and $Q_{delivered}$ depending on the concentration (Villarubia et al., 2016). However, the sensitivity resulted in a decrease both at a shorter and longer charging times. In the first case, the sensitivity drop could be ascribed to the short length of the charging time, while in the second case it can be related with the continuous voltage drop, which corresponds to a lower power density release over time (Santoro et al., 2019, 2016a).

4. Conclusions

In conclusion, we have presented an alternative approach to obtain a highly sensitive and stable self-powered biosensor that was used to detect fructose as proof of concept. By assembling charge-storing components with different capacitances and an FDH modified bioanode, we were able to increase the catalytic current density up to 8 times compared to the single biocatalytic electrode (FDH bioanode). Moreover, the proposed BSC showed promising features both in pulse mode and when applying a constant load, *viz.* a power density of 17.6 mW cm^{-2} and 3.8 mW cm^{-2}, respectively. Moreover, the power density achieved for the self-charging BSC in pulse mode or under constant load allowed the enhancement of sensitivity of the device up to ten times (3.82 ± 0.01 mW cm^{-2} mM^{-1}, charging time = 70 min) compared to the BSC in continuous operation and 100 times compared to the normal enzymatic fuel cell (EFC). The proposed BSC showed excellent biosensing features in terms of sensitivity (3.82 ± 0.01 mW cm^{-2} mM^{-1}) and operational stability (retaining up to 90% of its initial power density after 8 h of continuous operation). However, the present device exhibited a certain complexity (4 electrodes assembled to obtain the BSC), which hinders at the moment the *in-situ* detection of any analytically/biomedically relevant biomarker.

Acknowledgements

This work is part of the activities of the Johan Gadolin Process Chemistry Centre (PCC) at Åbo Akademi University. P.B. would like to acknowledge PCC for financial support in the form of a Johan Gadolin Scholarship. L.G. would like to thank the following agencies for financial support: The Swedish Research Council (Vetenskapsrådet project 2014-5908), the European Commission (project "Bioenergy" FP7-PEOPLE-2013-ITN- 607793). Z.B. is grateful to Jane and Aatos Erkko Foundation (project "New electrochemical sensing platforms for personalized medicine").

Author contributions

P.B. and Z.B. planned the conceptual and experimental work. R.M.L. supervised P.B. during the morphological and spectroscopic characterization. K.K. kindly donated samples of FDH from *Gluconobacter japonicus* (FDH; EC 1.1.99.11). P.B. wrote the manuscript. Z.B., R.M.L., K.K., L.G. and J.B. revised the manuscript. All the authors have read and approved the final version.

References

Abaci, S., Nessark, B., Riahi, F., 2014. Preparation and characterization of polyaniline+TiO_2 composite films. Ionics 20, 1693-1702.

Adachi, T., Kaida, Y., Kitazumi, Y., Shirai, O., Kano, K., 2019. Bioelectrocatalytic performance of d-fructose dehydrogenase. Bioelectrochemistry 129, 1–9.

Adachi, T., Kitazumi, Y., Shirai, O., Kano, K., 2020. Direct Electron Transfer-Type Bioelectrocatalysis of Redox Enzymes at Nanostructured Electrodes. Catalysts 10, art. No. 236.

Agnès, C., Holzinger, M., Le Goff, A., Reuillard, B., Elouarzaki, K., Tingry, S., Cosnier, S., 2014. Supercapacitor/biofuel cell hybrids based on wired enzymes on carbon nanotube matrices: autonomous reloading after high power pulses in neutral buffered glucose solutions. Energy Environ. Sci. 7, 1884-1888.

Alsaoub, S., Ruff, A., Conzuelo, F., Ventosa, E., Ludwig, R., Shleev, S., Schuhmann, W., 2017. An Intrinsic Self-Charging Biosupercapacitor Comprised of a High-Potential Bioanode and a Low-Potential Biocathode. ChemPlusChem 82, 576–583.

Bartlett, P.N., Birkin, P.R., 1993. The application of conducting polymers in biosensors. Synth. Met. 61, 15–21.

Bartonek, M., Sariciftci, N.S., Kuzmany, H., 1990. Resonance Raman spectroscopy of the emeraldine insulator-to-metal phase transition. Synth. Met. 36, 83–93.

Berrada, K., Quillard, S., Louam, G., Lefrant, S., 1995. Polyanilines and substituted polyanilines: a comparative study of the Raman spectra of leucoemeraldine, emeraldine and pernigraniline. Synth. Met. 69, 201–204.

Blanford, C.F., Foster, C.E., Heath, R.S., Armstrong, F.A., 2009. Efficient electrocatalytic oxygen reduction by the 'blue'copper oxidase, laccase, directly attached to chemically modified carbons. Faraday Discuss. 140, 319–335.

Bobrowski, T., González Arribas, E., Ludwig, R., Toscano, M.D., Shleev, S., Schuhmann, W., 2018. Rechargeable, flexible and mediator-free biosupercapacitor based on transparent ITO nanoparticle modified electrodes acting in μM glucose containing buffers. Biosens. Bioelectron. 101, 84-89.

Bollella, P., Fusco, G., Stevar, D., Gorton, L., Ludwig, R., Ma, S., Boer, H., Koivula, A., Tortolini, C., Favero, G., 2018a. A glucose/oxygen enzymatic fuel cell based on gold nanoparticles modified graphene screen-printed electrode. Proof-of-concept in human saliva. Sens. Actuators B Chem. 256, 921–930.

Bollella, P., Gorton, L., 2018. Enzyme based amperometric biosensors. Curr. Opin. Electrochem. 10, 157–173.

Bollella, P., Gorton, L., Antiochia, R., 2018b. Direct electron transfer of dehydrogenases for development of 3rd generation biosensors and enzymatic fuel cells. Sensors 18, art. No. 1319.

Bollella, P., Hibino, Y., Conejo-Valverde, P., Soto-Cruz, J., Bergueiro, J., Calderón, M., Rojas-Carrillo, O., Kano, K., Gorton, L., 2019. The influence of the shape of Au nanoparticles on the catalytic current of fructose dehydrogenase. Anal. Bioanal. Chem. 411, 7645–7657.

Bollella, P., Hibino, Y., Kano, K., Gorton, L., Antiochia, R., 2018c. Highly sensitive membraneless fructose biosensor based on fructose dehydrogenase immobilized onto aryl thiol modified highly porous gold electrode: characterization and application in food samples. Anal. Chem. 90, 12131–12136.

Bollella, P., Hibino, Y., Kano, K., Gorton, L., Antiochia, R., 2018d. Enhanced direct electron transfer of fructose dehydrogenase rationally immobilized on a 2-aminoanthracene

diazonium cation grafted single-walled carbon nanotube based electrode. ACS Catal. 8, 10279–10289.
Bollella, P., Hibino, Y., Kano, K., Gorton, L., Antiochia, R., 2018e. The influence of pH and divalent/monovalent cations on the internal electron transfer (IET), enzymatic activity, and structure of fructose dehydrogenase. Anal. Bioanal. Chem. 410, 3253–3264.
Brett, C.M., Thiemann, C., 2002. Conducting polymers from aminobenzoic acids and aminobenzenesulphonic acids: influence of pH on electrochemical behaviour. J. Electroanal. Chem. 538, 215–222.
Bulusheva, L.G., Okotrub, A.V., Kinloch, I.A., Asanov, I.P., Kurenya, A.G., Kudashov, A.G., Chen, X., Song, H., 2008. Effect of nitrogen doping on Raman spectra of multi-walled carbon nanotubes. Phys. Status Solidi B 245, 1971–1974.
Cao, Y., 1990. Spectroscopic studies of acceptor and donor doping of polyaniline in the emeraldine base and pernigraniline forms. Synth. Met. 35, 319-332.
Chiang, J.C., MacDiarmid, A.G., 1986. 'Polyaniline': protonic acid doping of the emeraldine form to the metallic regime. Synth. Met. 13, 193-205.
Conzuelo, F., Ruff, A., Schuhmann, W., 2018. Self-powered bioelectrochemical devices. Curr. Opin. Electrochem. 12, 156–163.
Costa, S., Borowiak-Palen, E., Kruszynska, M., Bachmatiuk, A., Kalenczuk, R.J., 2008. Characterization of carbon nanotubes by Raman spectroscopy. Mater. Sci.-Pol. 26, 433–441.
Falk, M., Blum, Z., Shleev, S., 2012. Direct electron transfer based enzymatic fuel cells. Electrochim. Acta 82, 191–202.
Fu, L., Liu, J., Hu, Z., Zhou, M., 2018. Recent Advances in the Construction of Biofuel Cells Based Self-powered Electrochemical Biosensors: A Review. Electroanalysis 30, 2535–2550.
Furukawa, Y., Ueda, F., Hyodo, Y., Harada, I., Nakajima, T., Kawagoe, T., 1988. Vibrational spectra and structure of polyaniline. Macromolecules 21, 1297–1305.
Fusco, G., Göbel, G., Zanoni, R., Kornejew, E., Favero, G., Mazzei, F., Lisdat, F., 2017. Polymer-supported electron transfer of PQQ-dependent glucose dehydrogenase at carbon nanotubes modified by electropolymerized polythiophene copolymers. Electrochim. Acta 248, 64–74.
Gonzalez-Arribas, E., Aleksejeva, O., Bobrowski, T., Toscano, M.D., Gorton, L., Schuhmann, W., Shleev, S., 2017. Solar biosupercapacitor. Electrochem. Commun. 74, 9–13.
Gorton, L., 2020. Special Issue on Sugar Oxidising Enzymes. Bioelectrochemistry 134, art. No. 107577
Grattieri, M., Minteer, S.D., 2018. Self-powered biosensors. ACS Sens. 3, 44–53.
Heise, H.M., Kuckuk, R., Ojha, A.K., Srivastava, A., Srivastava, V., Asthana, B.P., 2009. Characterisation of carbonaceous materials using Raman spectroscopy: a comparison of carbon nanotube filters, single-and multi-walled nanotubes, graphitised porous carbon and graphite. J. Raman Spectrosc. 40, 344–353.
Heller, A., 1992. Electrical connection of enzyme redox centers to electrodes. J. Phys. Chem. 96, 3579–3587.
Hickey, D.P., Reid, R.C., Milton, R.D., Minteer, S.D., 2016. A self-powered amperometric lactate biosensor based on lactate oxidase immobilized in dimethylferrocene-modified LPEI. Biosens. Bioelectron. 77, 26–31.
Houghton, J., Santoro, C., Soavi, F., Serov, A., Ieropoulos, I., Arbizzani, C., Atanassov, P., 2016. Supercapacitive microbial fuel cell: characterization and analysis for improved charge storage/delivery performance. Bioresour. Technol. 218, 552–560.
Huang, W.S., Humphrey, B.D., MacDiarmid, A.G., 1986. Polyaniline, a novel conducting polymer. Morphology and chemistry of its oxidation and reduction in aqueous electrolytes. J. Chem. Soc., Faraday Trans. 1 82, 2385-2400.

Kamitaka, Y., Tsujimura, S., Setoyama, N., Kajino, T., Kano, K., 2007. Fructose/dioxygen biofuel cell based on direct electron transfer-type bioelectrocatalysis. Phys. Chem. Chem. Phys. 9, 1793–1801.

Karami, H., Asadi, M.G., Mansoori, M., 2012. Pulse electropolymerization and the characterization of polyaniline nanofibers. Electrochim. Acta 61, 154–164.

Katz, E., Bückmann, A.F., Willner, I., 2001. Self-powered enzyme-based biosensors. J. Am. Chem. Soc. 123, 10752–10753.

Kizling, M., Draminska, S., Stolarczyk, K., Tammela, P., Wang, Z., Nyholm, L., Bilewicz, R., 2015. Biosupercapacitors for powering oxygen sensing devices. Bioelectrochemistry 106, 34–40.

Kizling, M., Stolarczyk, K., Tammela, P., Wang, Z., Nyholm, L., Golimowski, J., Bilewicz, R., 2016. Bioelectrodes based on pseudocapacitive cellulose/polypyrrole composite improve performance of biofuel cell. Bioelectrochemistry 112, 184–190.

Leech, D., Kavanagh, P., Schuhmann, W., 2012. Enzymatic fuel cells: Recent progress. Electrochim. Acta 84, 223–234.

Liang, P., Huang, X., Fan, M.-Z., Cao, X.-X., Wang, C., 2007. Composition and distribution of internal resistance in three types of microbial fuel cells. Appl. Microbiol. Biotechnol. 77, 551–558.

Lindfors, T., Ivaska, A., 2002. pH sensitivity of polyaniline and its substituted derivatives. J. Electroanal. Chem. 531, 43–52.

Lindfors, T., Latonen, R.-M., 2014. Improved charging/discharging behavior of electropolymerized nanostructured composite films of polyaniline and electrochemically reduced graphene oxide. Carbon 69, 122–131.

Lisdat, F., 2020. PQQ-GDH–Structure, function and application in bioelectrochemistry. Bioelectrochemistry 134, art. No. 107496.

Mano, N., 2019. Engineering glucose oxidase for bioelectrochemical applications. Bioelectrochemistry 128, 218–240.

Momeni, M.H., Bollella, P., Ortiz, R., Thormann, E., Gorton, L., Abou Hachem, M., 2019. A novel starch-binding laccase from the wheat pathogen Zymoseptoria tritici highlights the functional diversity of ascomycete laccases. BMC Biotechnol. 19, art. No. 61.

Okuda-Shimazaki, J., Yoshida, H., Sode, K., 2020. FAD dependent glucose dehydrogenases–Discovery and engineering of representative glucose sensing enzymes. Bioelectrochemistry 132, art. No. 107414.

Pankratov, D., Blum, Z., Suyatin, D.B., Popov, V.O., Shleev, S., 2014a. Self-Charging Electrochemical Biocapacitor. ChemElectroChem 1, 343–346.

Pankratov, D., Conzuelo, F., Pinyou, P., Alsaoub, S., Schuhmann, W., Shleev, S., 2016. A nernstian biosupercapacitor. Angew. Chem. Int. Ed. 55, 15434–15438.

Pankratov, D., Falkman, P., Blum, Z., Shleev, S., 2014b. A hybrid electric power device for simultaneous generation and storage of electric energy. Energy Environ. Sci. 7, 989–993.

Pankratov, D., Shen, F., Ortiz, R., Toscano, M.D., Thormann, E., Zhang, J., Gorton, L., Chi, Q., 2018. Fuel-independent and membrane-less self-charging biosupercapacitor. Chem. Commun. 54, 11801–11804.

Pankratova, G., Pankratov, D., Hasan, K., Åkerlund, H.-E., Albertsson, P.-Å., Leech, D., Shleev, S., Gorton, L., 2017. Supercapacitive Photo-Bioanodes and Biosolar Cells: A Novel Approach for Solar Energy Harnessing. Adv. Energy Mater. 7, Art. No. 1602285.

Peterbauer, C.K., 2020. Pyranose dehydrogenases: Rare enzymes for electrochemistry and biocatalysis. Bioelectrochemistry 132, art. No. 107399.

Quillard, S., Berrada, K., Louarn, G., Lefrant, S., Lapkowski, M., Pron, A., 1995. *In situ* Raman spectroscopic studies of the electrochemical behavior of polyaniline. New J. Chem. 19, 365–374.

Rahy, A., Yang, D.J., 2008. Synthesis of highly conductive polyaniline nanofibers. Mater. Lett. 62, 4311-4314.
Ramanavičius, A., Ramanavičienė, A., Malinauskas, A., 2006. Electrochemical sensors based on conducting polymer—polypyrrole. Electrochim. Acta 51, 6025–6037.
Roy, B.G., Rutherford, J.L., Weaver, A.E., Beaver, K., Rasmussen, M., 2020. A Self-Powered Biosensor for the Detection of Glutathione. Biosensors, 10 (9), art. No. 114.
Ruff, A., 2017. Redox polymers in bioelectrochemistry: Common playgrounds and novel concepts. Curr. Opin. Electrochem. 5, 66–73.
Santoro, C., Soavi, F., Arbizzani, C., Serov, A., Kabir, S., Carpenter, K., Bretschger, O., Atanassov, P., 2016a. Co-generation of hydrogen and power/current pulses from supercapacitive MFCs using novel HER iron-based catalysts. Electrochim. Acta 220, 672–682.
Santoro, C., Soavi, F., Serov, A., Arbizzani, C., Atanassov, P., 2016b. Self-powered supercapacitive microbial fuel cell: the ultimate way of boosting and harvesting power. Biosens. Bioelectron. 78, 229–235.
Santoro, C., Walter, X.A., Soavi, F., Greenman, J., Ieropoulos, I., 2019a. Self-stratified and self-powered micro-supercapacitor integrated into a microbial fuel cell operating in human urine. Electrochim. Acta 307, 241–252.
Santoro, C., Pankratov, D., Ieropoulos, I., Soavi, F., 2019b. Bioelectrochemistry: Design and Applications of Biomaterials. Walter de Gruyter GmbH & Co KG, Berlin/Boston, 189-212.
Scheiblbrandner, S., Ludwig, R., 2020. Cellobiose dehydrogenase: Bioelectrochemical insights and applications. Bioelectrochemistry 131, art. No. 107345.
Schubart, I.W., Göbel, G., Lisdat, F., 2012. A pyrroloquinolinequinone-dependent glucose dehydrogenase (PQQ-GDH)-electrode with direct electron transfer based on polyaniline modified carbon nanotubes for biofuel cell application. Electrochim. Acta 82, 224–232.
Schuhmann, W., Kranz, C., Wohlschläger, H., Strohmeier, J., 1997. Pulse technique for the electrochemical deposition of polymer films on electrode surfaces. Biosens. Bioelectron. 12, 1157–1167.
Shleev, S., 2017. Quo vadis, implanted fuel cell? ChemPlusChem 82, 522–539.
Shleev, S., Gonzalez-Arribas, E., Falk, M., 2017. Biosupercapacitors. Curr. Opin. Electrochem. 5, 226–233.
Shleev, S., Tkac, J., Christenson, A., Ruzgas, T., Yaropolov, A.I., Whittaker, J.W., Gorton, L., 2005. Direct electron transfer between copper-containing proteins and electrodes. Biosens. Bioelectron. 20, 2517–2554.
So, K., Kawai, S., Hamano, Y., Kitazumi, Y., Shirai, O., Hibi, M., Ogawa, J., Kano, K., 2014. Improvement of a direct electron transfer-type fructose/dioxygen biofuel cell with a substrate-modified biocathode. Phys. Chem. Chem. Phys. 16, 4823–4829.
Soavi, F., Santoro, C., 2020. Supercapacitive operational mode in microbial fuel cell. Curr. Opin. Electrochem. 22, 1–8.
Villarrubia, C.W.N., Soavi, F., Santoro, C., Arbizzani, C., Serov, A., Rojas-Carbonell, S., Gupta, G., Atanassov, P., 2016. Self-feeding paper based biofuel cell/self-powered hybrid μ-supercapacitor integrated system. Biosens. Bioelectron. 86, 459–465.
Wiklund, P., Bergman, J., 2006. The chemistry of anthranilic acid. Curr. Org. Synth. 3, 379–402.
Xiao, X., Magner, E., 2018. A quasi-solid-state and self-powered biosupercapacitor based on flexible nanoporous gold electrodes. Chem. Commun. 54, 5823–5826.
Xiao, X., Xia, H., Wu, R., Bai, L., Yan, L., Magner, E., Cosnier, S., Lojou, E., Zhu, Z., Liu, A., 2019. Tackling the challenges of enzymatic (bio) fuel cells. Chem. Rev. 119, 9509–9558.

Yang, Y., Zhang, H., Chen, J., Lee, S., Hou, T.-C., Wang, Z.L., 2013. Simultaneously harvesting mechanical and chemical energies by a hybrid cell for self-powered biosensors and personal electronics. Energy Environ. Sci. 6, 1744–1749.

Yoon, S.B., Yoon, E.H., Kim, K.B., 2011. Electrochemical properties of leucoemeraldine, emeraldine, and pernigraniline forms of polyaniline/multi-wall carbon nanotube nanocomposites for supercapacitor applications. J. Power Sources 196, 10791-10797.

Yuan, M., Minteer, S.D., 2019. Redox polymers in electrochemical systems: From methods of mediation to energy storage. Curr. Opin. Electrochem. 15, 1–6.

Zamani, F.G., Moulahoum, H., Ak, M., Demirkol, D.O., Timur, S., 2019. Current trends in the development of conducting polymers-based biosensors. TrAC Trends Anal. Chem. 118, 264–276.

Zumpano, R., Lambertini, L., Tortolini, C., Bollella, P., Favero, G., Antiochia, R., Mazzei, F., 2020. A glucose/oxygen enzymatic fuel cell exceeding 1.5 V based on glucose dehydrogenase immobilized onto polyMethylene blue-carbon nanotubes modified double-sided screen printed electrodes: Proof-of-concept in human serum and saliva. J. Power Sources 476, art. No. 228615.

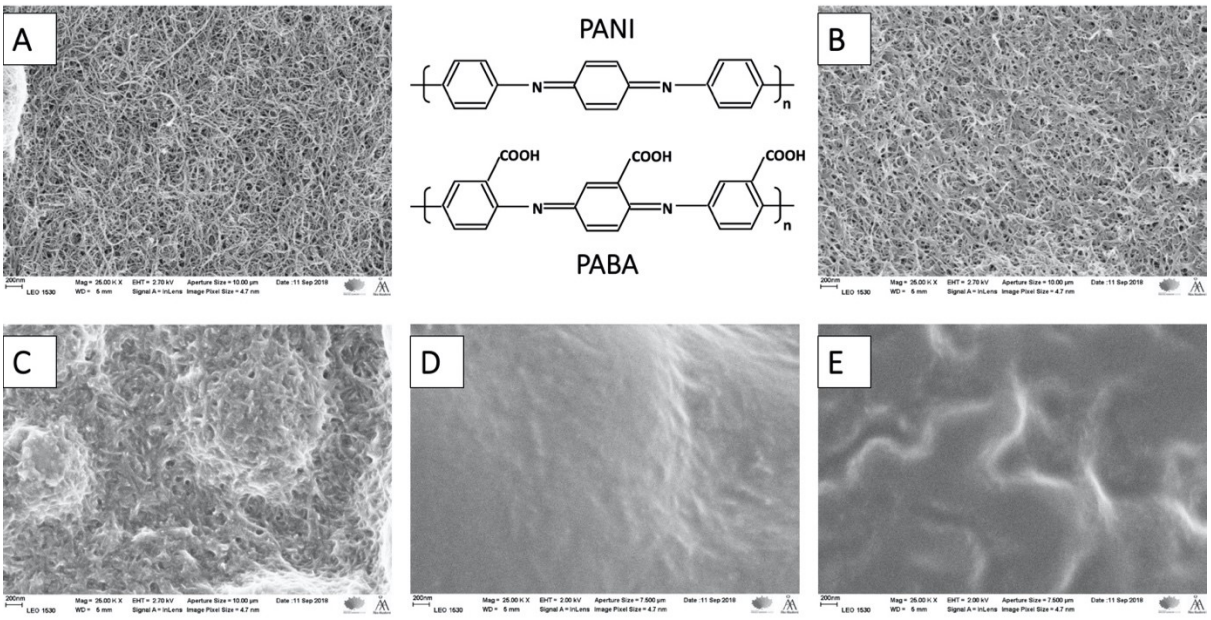

Figure 1. The chemical structures for PANI and PABA and SEM images of (**A**) MWCNT/G (accelerating voltage: 2.7 kV), (**B**) PABA/MWCNT/G, (**C**) PANI/MWCNT/G with t_{exp}= 200 s, (**D**) PANI/MWCNT/G with t_{exp}= 400 s and (**E**) PABA/MWCNT/G with t_{exp}= 600 s (only for D and E accelerating voltage: 2.0 kV).

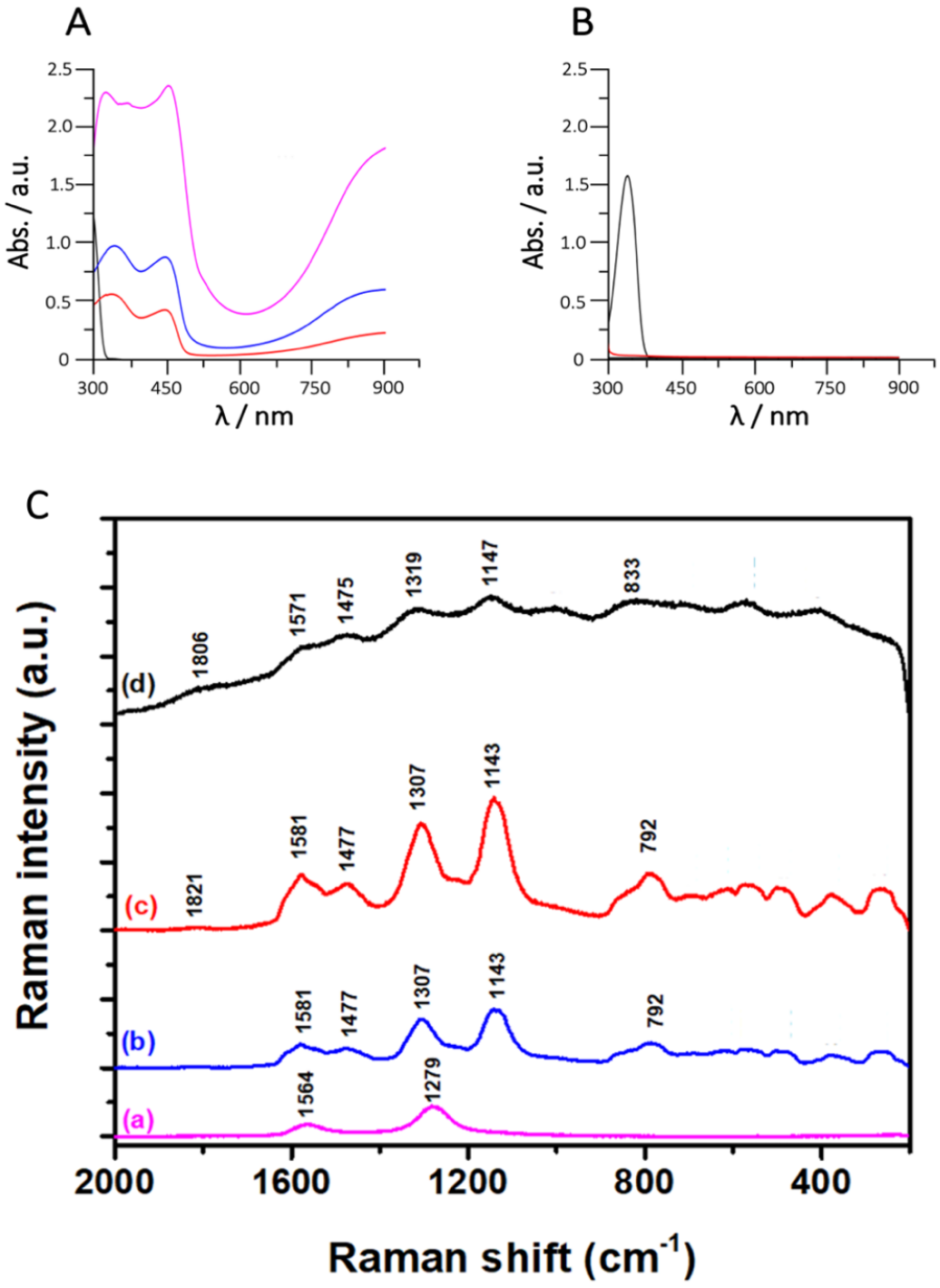

Figure 2. (A) UV-Vis spectra of PANI electropolymerized onto ITO electrodes in 1 M H_2SO_4: aniline monomer (black curve), PANI t_{exp}= 200 s (red curve), PANI t_{exp}= 400 s (blue curve) and PANI t_{exp}= 600 s (magenta curve); Optimal experimental conditions of PANI electropolymerization: [ANI]= 0.1 M, E_{ox}=0.9 V vs. Ag|AgCl (3M KCl), t_{ox}= 0.4 s, E_{red}= -0.1 V vs. Ag|AgCl (3M KCl), t_{red}= 0.2 s and t_{exp}= 300 s. **(B)** PABA electropolymerized onto ITO electrodes in 1 M H_2SO_4: 2-aminobenzoic acid monomer (black curve), PABA t_{exp}= 300 s (red curve). Optimal experimental conditions of PABA electropolymerization: [ABA]= 0.1 M, E_{ox}=0.7 V vs. Ag|AgCl (3M KCl), t_{ox}= 0.4 s, E_{red}= -0.1 V vs. Ag|AgCl (3M KCl), t_{red}= 0.2 s and t_{exp}= 300 s. **(C)** Raman spectra of (**a**, magenta curve) MWCNT/G, λ_{exc}=514 nm, (**b**, blue curve) PANI t_{exp}= 200 s/MWCNT/G, (**c**, red curve) PANI t_{exp}= 400 s/MWCNT/G and (**d**, black curve) PANI t_{exp}= 600 s /MWCNT/G, λ_{exc}=784 nm for PANI/MWCNT/G.

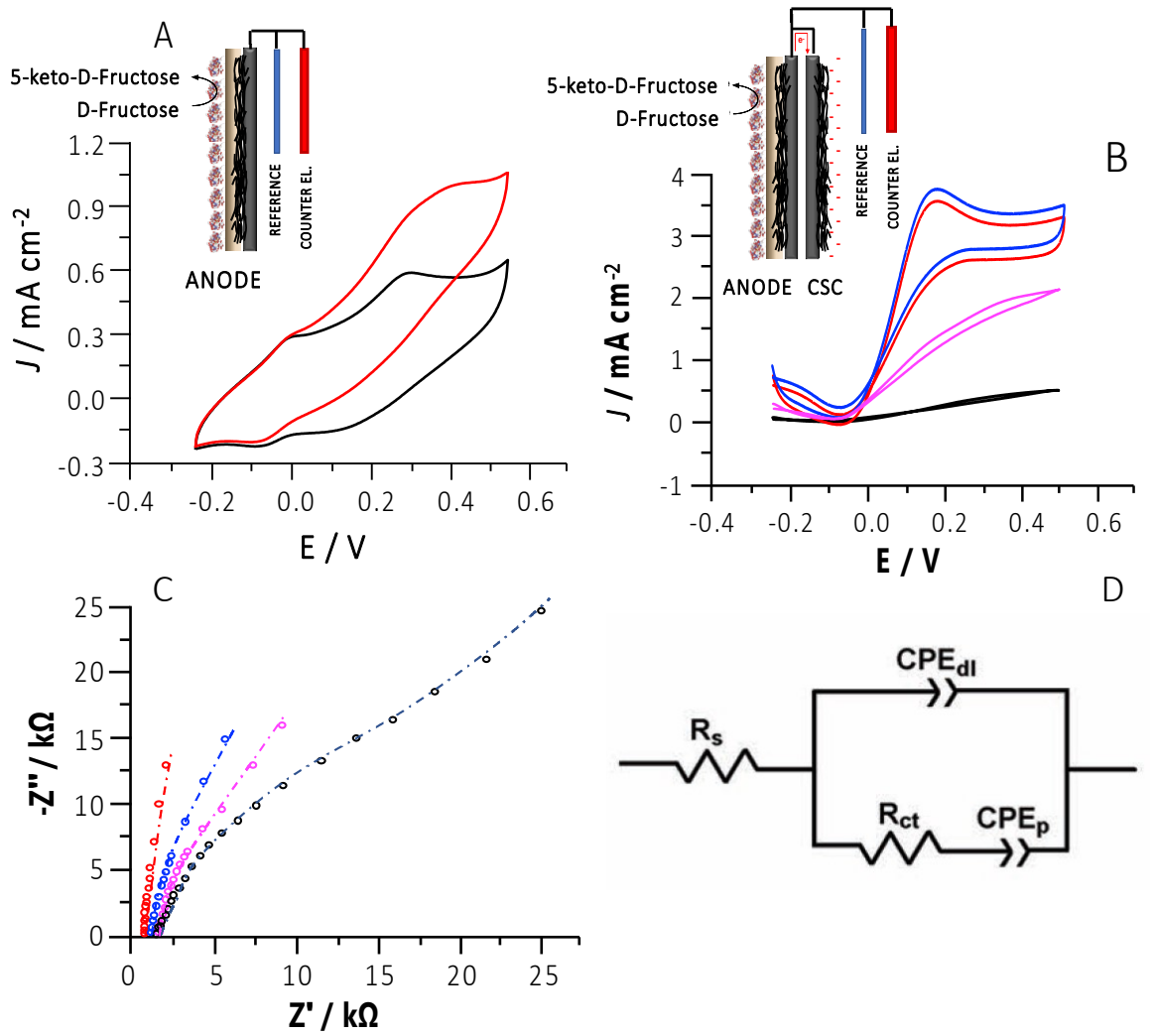

Figure 3. (A) CVs of FDH/PABA/MWCNT/G in absence (black curve) and in presence of 10 mM D-Fructose (red curve). **(B)** Subtracted CVs for FDH/PABA/MWCNT/G supercapacitive electrode (SCP, black curve) and SCP containing charge storing components (CSCs) of 0.5 (magenta curve), 1.2 (blue curve) and 2 (red curve) mF in presence of 10 mM D-Fructose. Experimental conditions: 50 mM NaAc buffer at pH 5, scan rate 5 mV s^{-1}, T = 25 ºC. **(C)** Experimental (dots) and modeled (dashed curves) Nyquist plots at 0.4 V for FDH/PABA/MWCNT/G supercapacitive electrode (SCP, black curve) and SCP containing CSCs of 0.5 (magenta curve), 1.2 (blue curve) and 2 (red curve) mF. **(D)** Equivalent circuit model used to fit the EIS spectra reported in **(C)**.

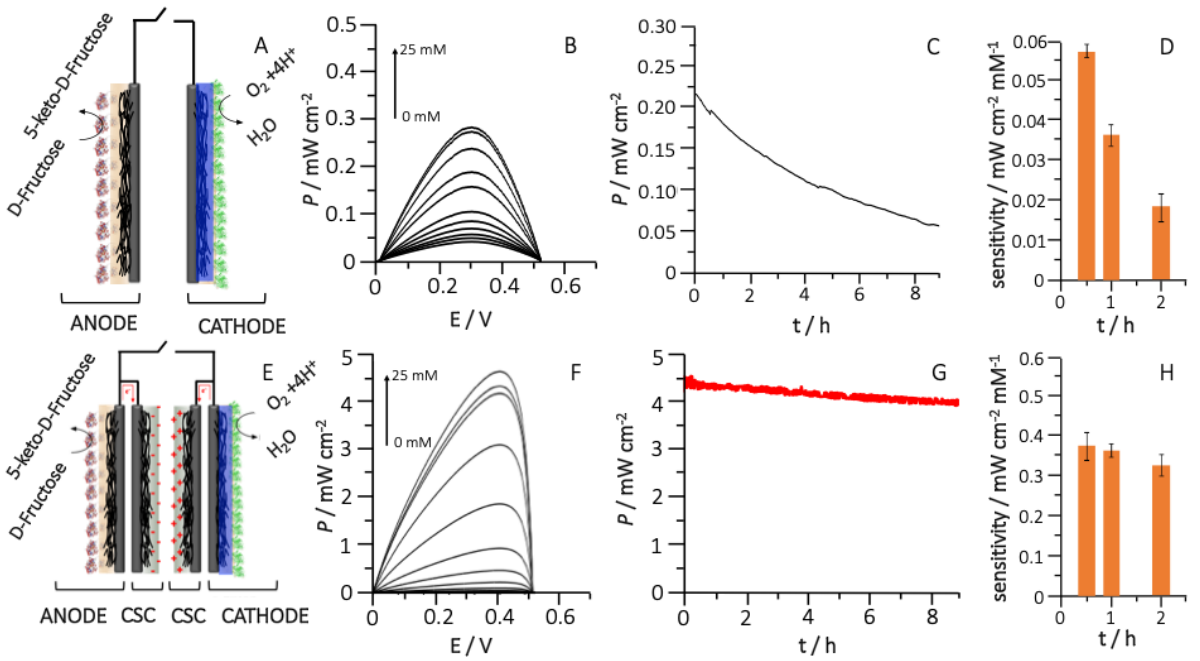

Figure 4. (A) Schematic representation of EFC: FDH/PABA/MWCNT/G||G/MWCNT/2-ANT/TvL **(B)** Power output profiles recorded for FDH/PABA/MWCNT/G||G/MWCNT/2-ANT/TvL EFC in 50 mM NaAc buffer pH 5 containing different concentrations of D-Fructose from 0 mM up to 25 mM and in equilibrium with air (source of O_2). The plot was obtained from linear sweep voltammetry at 1 mV s^{-1}. **(C)** Power output trend of EFC upon 8 working hours applying a constant load of 250 Ω. **(D)** Sensitivity calculated from the calibration curve measured for the EFC working as self-powered biosensor upon operation time. **(E)** Schematic representation of BSC: FDH/PABA/MWCNT/G-CSC||CSC-G/MWCNT/2-ANT/TvL **(F)** Power output profiles recorded for FDH/PABA/MWCNT/G-CSC||CSC-G/MWCNT/2-ANT/TvL BSC in 50 mM NaAc buffer pH 5 containing different concentrations of D-Fructose from 0 mM up to 25 mM and in equilibrium with air (source of O_2). The plot was obtained from linear sweep voltammetry at 1 mV s^{-1}. **(G)** Power output trend of BSC upon 8 working hours applying a constant load of 250 Ω. (H) Sensitivity calculated from the calibration curve measured for the BSC working as self-powered biosensor upon operation time.

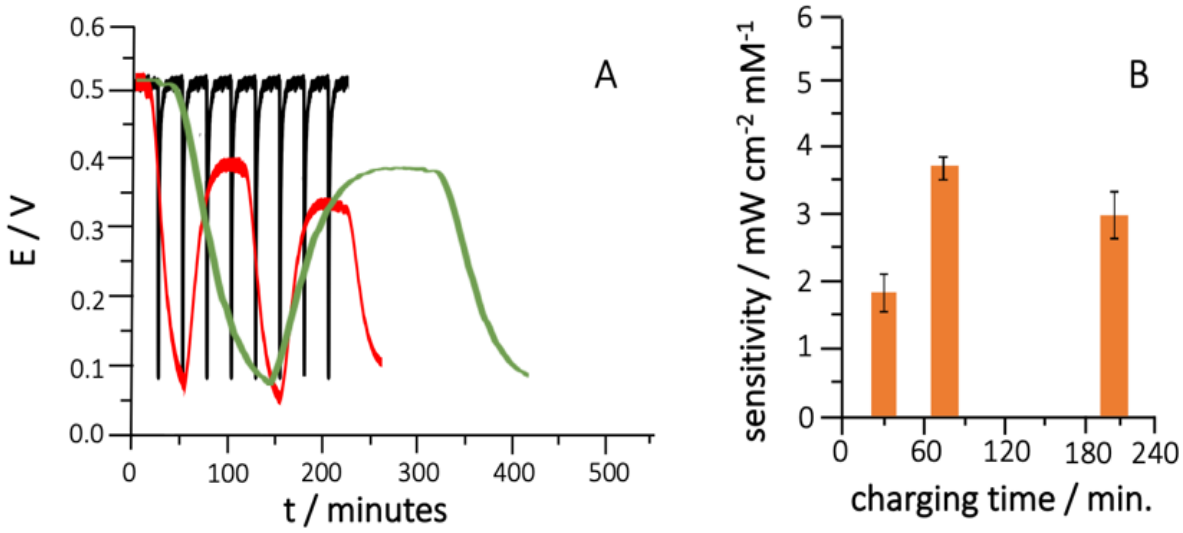

Figure 5. (A) Charge/discharge curve of self-charging FDH/PABA/MWCNT/G-CSC||CSC-G/MWCNT/2-ANT/TvL BSC; discharge was carried out by applying a pulse current of 100 µA for 3 s (black curve), constant load of 250 Ω for 50 mins and self-charging for 70 mins. (red curve), constant load of 250 Ω for 100 mins and self-charging for 200 mins. (green curve). Experimental conditions: 50 mM NaAc pH 5 containing 20 mM D-Fructose and air-equilibrated. **(B)** Sensitivity calculated from the calibration curve measured for the self-charging BSC working as self-powered biosensor upon different charging times.

Graphical Abstract

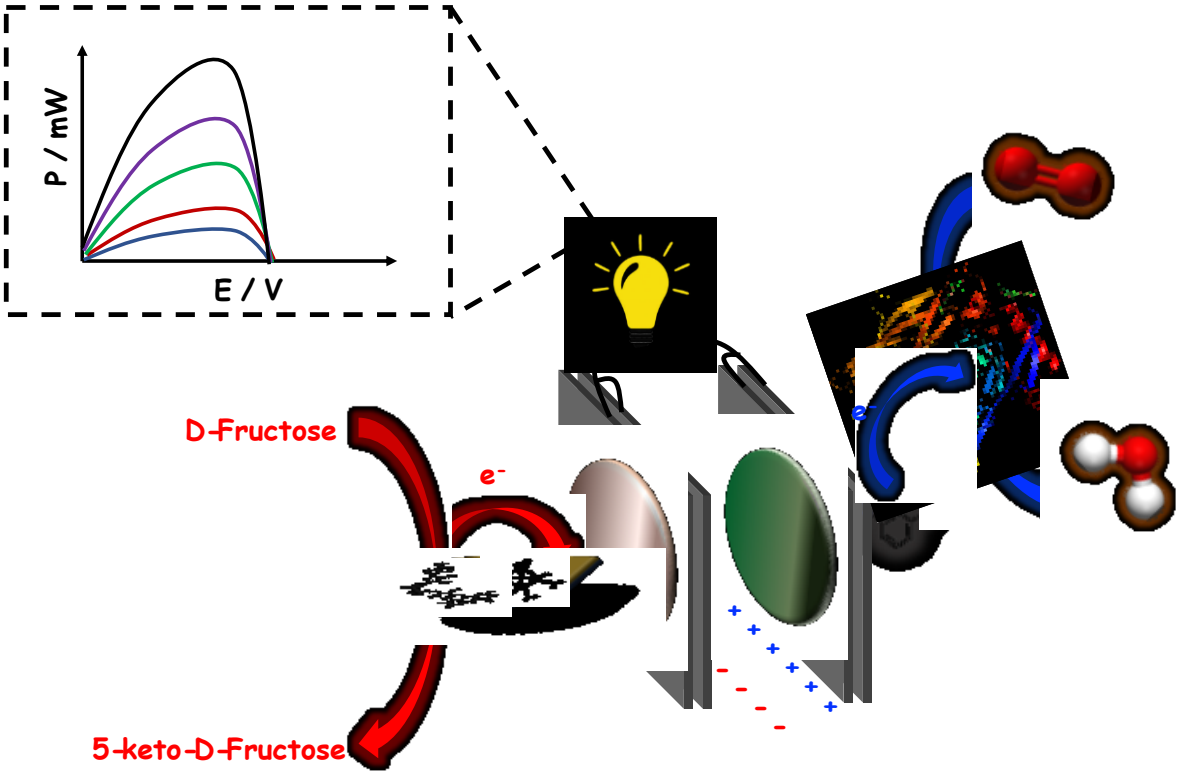

A new fructose dehydrogenase (FDH) based self-charging biosupercapacitor has been developed as a self-powered biosensor in order to increase the device sensitivity by 100 times compared to a similar device operating as enzymatic fuel cell (EFC). This is a novel approach in "smart-biosensing" that could be potentially integrated with flexible supports for food and biomedical applications.